Front. Phys. 13(5), 136803 (2018)
https://doi.org/10.1007/s11467-018-0819-6

RESEARCH ARTICLE

Ferroelectric polarization reversal tuned by magnetic field in a ferroelectric $BiFeO_3$/Nb-doped $SrTiO_3$ heterojunction

Pei Li[1], Zhao-Meng Gao[1], Xiu-Shi Huang[1], Long-Fei Wang[1], Wei-Feng Zhang[1,†], Hai-Zhong Guo[1,2,‡]

[1] *Henan Key Laboratory of Photovoltaic Materials, School of Physics and Electronics, Henan University, Kaifeng 475004, China*
[2] *School of Physical Engineering, Zhengzhou University, Zhengzhou 450001, China*
Corresponding authors. E-mail: †wfzhang6@163.com, ‡hguo@zzu.edu.cn
Received April 11, 2018; accepted June 15, 2018

Interfacial resistive switching of a ferroelectric semiconductor heterojunction is highly advantageous for the newly developed ferroelectric memristors. Moreover, the interfacial state in the ferroelectric semiconductor heterojunction can be gradually modified by polarization reversal, which may give rise to continuously tunable resistive switching behavior. In this work, the interfacial state of a ferroelectric $BiFeO_3$/Nb-doped $SrTiO_3$ junction was modulated by ferroelectric polarization reversal. The dynamics of surface screening charges on the $BiFeO_3$ layer was also investigated by surface potential measurements, and the decay of the surface potential could be speeded up by the magnetic field. Moreover, ferroelectric polarization reversal of the $BiFeO_3$ layer was tuned by the magnetic field. This finding could provide a method to enhance the ferroelectric and electrical properties of ferroelectric $BiFeO_3$ films by tuning the magnetic field.

Keywords ferroelectric semiconductor heterojunction, ferroelectric polarization reversal, pulsed laser deposition, Kelvin probe force microscopy

PACS numbers 68.37.Ps, 77.80.Fm, 77.55.Nv

$BiFeO_3$ (BFO), which is used as both a ferroelectric and an antiferromagnetic material in new magnetoelectric and magneto-optical devices, has broad prospects for application in devices such as nonvolatile memory, field-effect transistors, and magnetoelectric switches [1–3]. In recent years, many experimental and theoretical methods have been used to deeply investigate the structural, ferroelectric, and electrical properties of BFO under different experimental conditions, such as doping, laser, domain scales [4–7]. BFO films generally exhibit *p*-type conducting behavior as a result of Bi loss. Therefore, a Schottky junction or a *p*–*n* junction may be formed at the metal/BFO interface or the BFO/*n*-type semiconductor interface, respectively [8]. These junctions can be modulated by the ferroelectric polarization, which induces blocking or non-blocking interfaces for carrier transport, and thus resistive switching behavior [9]. In contrast to that in a conventional heterostructure, the interfacial state in a ferroelectric semiconductor heterojunction can be gradually modified by polarization reversal, which may give rise to continuously tunable resistive switching behavior [10]. Because polarization reversal is more stable than chemical alteration and is intrinsically fast, interfacial resistive switching is highly advantageous for the newly developed ferroelectric memristors.

In this work, a BFO/Nb-doped $SrTiO_3$ (NSTO) ferroelectric heterojunction was fabricated by pulsed laser deposition (PLD). Various advanced and powerful techniques based on atomic force microscopy (AFM, Asylum Research MFP-3D Infinity), such as piezoresponse force microscopy (PFM), electric force microscopy (EFM), surface Kelvin probe force microscopy (KPFM), and conductive AFM (CAFM), were used to characterize the local domain structure and microelectrical properties of the ferroelectric BFO/NSTO heterojunction. A magnetic field was introduced to modulate the ferroelectric polarization, and the influence of the magnetic field on the ferroelectric properties (domain structure and piezoresponse) and electrical characteristics [surface charge density, surface potential (SP), and charge conductivity] were investigated through imaging observations.

The BFO/NSTO heterojunction was fabricated by depositing a BFO layer on the NSTO substrate by PLD using a KrF excimer laser at a wavelength of 248 nm. BFO

ceramic targets with Bi/Fe ratios of 1:1 were made by mixing, grinding, pressing, and sintering. The distance between the target and substrate was kept at 70 mm. The growth temperature was kept at 670°C, and the oxygen pressure was 0.1 Torr. The frequency and energy density of the laser were 2 Hz and 1.5 J/cm^2, respectively. After 20 min of deposition, the films were slowly cooled to room temperature under a high oxygen ambient pressure (approximately 1 Torr). The thickness of the BFO layer is approximately 60 nm, as measured by a scanning electron microscope (SEM) technique; a cross-sectional SEM image is shown in Fig. 1. The growth method is described in detail in our previous work [11, 12].

The surface topographies were measured using an AFM (Asylum Research MFP-3D Infinity) with a closed loop controller. The ferroelectric switching properties were investigated via PFM, and the electrical properties were studied via EFM and KPFM while focusing on the same area of the film and using conductive Ti/Ir (5/20)-coated silicon tips. In PFM mode, the amplitude of the AC read voltage applied to the tip was 1 V. The ferroelectric phase and amplitude hysteresis loops versus the tip bias were measured in fixed locations on the film surface as a function of the DC switching bias superimposed on the AC modulation bias with a sweep voltage of 0 V $\rightarrow$ +9 V $\rightarrow$ −9 V $\rightarrow$ 0 V. For the KPFM measurement, the probe, at an AC voltage of 1 V, was also fixed 30 nm above the film surface. A surface topography image of the BFO layer is shown in Fig. 2(a). The BFO layer is flat and uniform, and the surface roughness is in the range of a few nanometers. Nanometer-scale polarization patterning can be achieved by the PFM technique. A polarization pattern with contrasting polarization can be created by flipping the tip bias during scanning with a tip-bias voltage larger than the coercive voltage to obtain well-defined domains with opposite polarization, as demonstrated in the out-of-plane PFM phase image shown in Fig. 2(b). The violet regions correspond to downward-polarized domains, and the yellow regions correspond to upward-polarized domains with the same polarization direction as the as-grown BFO/NSTO heterojunction [13]. The BFO layer clearly has good ferroelectric quality, and the asymmetric coercive fields from the local piezoresponse phase hysteresis are shown in Fig. 2(d). The associated voltage fields are $E_C(+) = 4$ V and $E_C(-) = -3$ V, respectively. After the polarization is switched to the downward direction by applying a positive voltage to the conductive tip, positive screening charges are accumulated on the surface of a domain. In contrast, negative screening charges are accumulated on the surface after the polarization is switched to the upward direction [14].

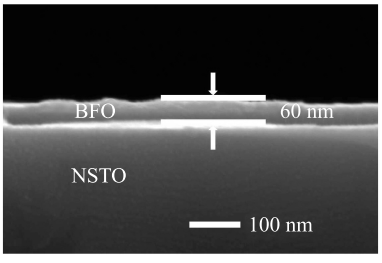

Fig. 1 The SEM cross-section image of the BFO/NSTO heterostructure.

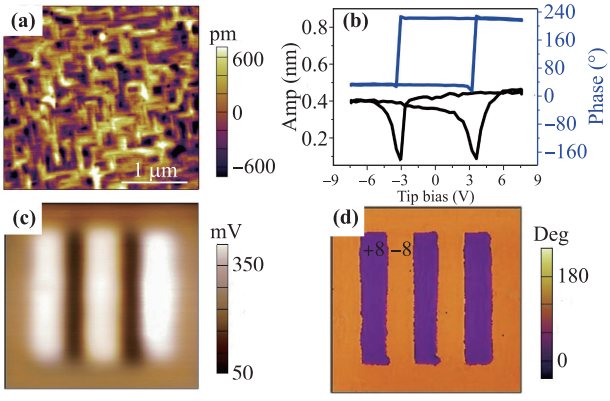

Fig. 2 **(a)** The virgin AFM topography. **(b)** The PFM phase image written by the PFM tip with +8 V and −8 V bias, respectively. **(c)** The corresponding KPFM image at the same area obtained as (b). **(d)** The phase and amplitude hysteresis of the BFO layer.

As the readout signal for the contrasting polarization domains, SP can be quantitatively obtained by the KPFM technique. KPFM was used to study the surface charge dynamics by imaging the surface screening charge distribution. Figure 2(c) shows a KPFM image of the patterned area shown in Fig. 2(b); both images were obtained immediately after sample poling. The difference in imaging contrast reflects the *SP* difference of the patterned domains. As shown in Fig. 2(c), a larger SP (white regions) is observed over the downward-polarized domains, whereas a smaller SP (black regions) is observed over the upward-polarized domains, indicating that the value of the domain-related SP is governed by the screening charges [4, 5]. All SP values on the BFO layer are positive regardless of the sign of the applied voltage, which may be related to the choice of the zero point of SP or the nonzero SP in the as-grown BFO layers.

SP decayed with time, and this decay can be speeded up by the magnetic field. Figures 3(a)–(h) summarize the results of the KPFM potential images and the time-dependence of the SP profiles under different magnetic fields. Figures 3(a)–(c) show KPFM images taken for approximately 15 h beginning immediately after poling [7]. High and low SP correspond to tip-injected positive and negative over-screened surface charges on the downward-

polarized and upward-polarized domains, respectively [15]. This over-screening effect after tip-induced switching is identical with that in previous reports [16]. The SP obviously undergoes different degrees of decay with time under the same magnetic field [5]. However, when the magnetic field is 7000 Oe, SP is almost unchanged after 15 h. In contrast, at $H = 0$ Oe, for the same decay time, there are obvious changes in SP. We can directly understand the decay phenomenon from Figs. 3(a)–(f). It is easy to understand that there are more screening charges on the surface of the domains at $H = 7000$ Oe 15 h after the sample was polarized; therefore, the initial values of the change in SP are larger. To quantitatively assess the dynamics of the SP in the reversed domains, Figs. 3(d)–(f) show line profiles of the KPFM images at different times and under different magnetic fields after the BFO/NSTO heterojunction was polarized. SP obviously decreases in the regions with high SP and increases in the regions with low SP. Therefore, ΔSP decays with time under different magnetic fields. Here, we defined ΔSP as the difference in SP between oppositely polarized domains. We attribute this decay to the reduction in tip-injected over-screened charges. It is easy to understand that there are screening charges on the surface of both the upward-polarized and downward-polarized domains, and the width of the initial surface density of the screening charges is almost the same as the domain width, because the duration and magnitude of the bias are uniform throughout the poling process. Interestingly, ΔSP decays much more rapidly at $H = 0$ Oe than at $H = 7000$ Oe. In other words, the magnetic field strongly influences ΔSP. To compare the decay dynamics under different magnetic fields, we normalized the values of ΔSP in Fig. 3(g) and plotted the time evolution of the normalized ΔSP in Fig. 3(h). From Fig. 3(g), we cannot plot the ΔSP ($H = 7000$ Oe) points after 15 h of decay because the KPFM potential image of the striped domains was obscure, and the domains could not be distinguished after poling. ΔSP ($H = 0$ Oe) is very close to zero 15 h after poling. We find that the time constant increases under the larger magnetic field. When the magnetic field is larger, the screening charges need to diffuse over a shorter time to recombine, and therefore it takes less time for ΔSP to decay. The trapping effect from the dipoles and the potential barrier (approximately 0.3 eV) at domain boundaries will hinder diffusion of the surface charges and cause ΔSP to decay to a stable value. Further, we believe that the tip-injected charge began to diffuse sideways once the tip contacted the surface under an applied bias. Therefore, we can conclude that the number of over-screened charges decreases more rapidly in the region with the same domains under different magnetic fields [17]. Figure 3 shows that the polarization reversal domain under the same voltage will show different changes with time. Therefore, we can conclude that the number of over-screened charges decreases more slowly in the region under higher magnetic fields.

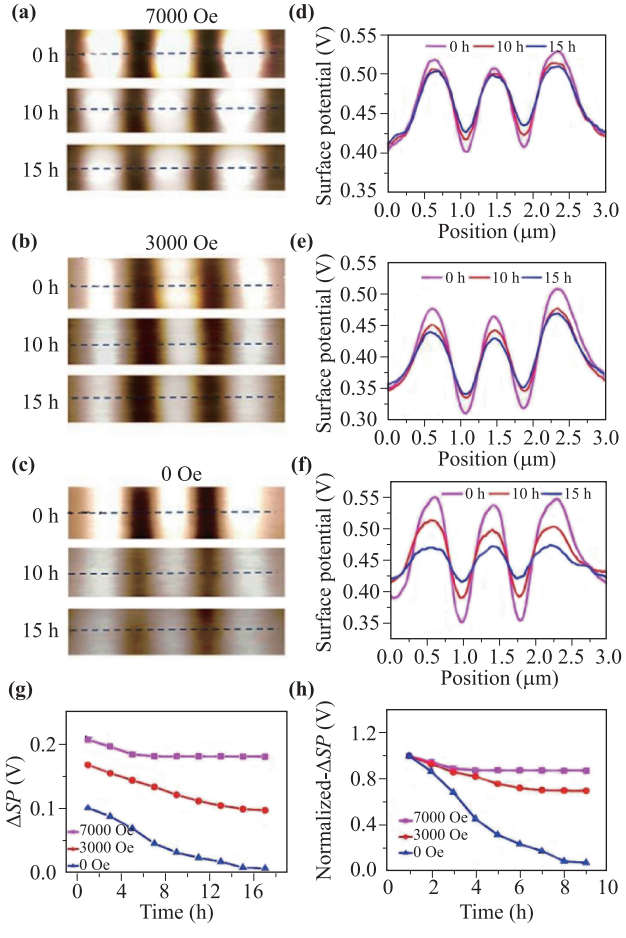

Fig. 3 The time dependences of **(a–c)** the KPFM images and **(d–f)** the responding surface potential profiles for the BFO layer under the different magnetic fields of 7000, 3000, and 0 Oe, respectively. **(h)** The time dependences of nomalized-ΔSP for the BFO layers. The solid lines represent the fitting curves to an exponential decay function.

To further explore the influence of the magnetic field on the surface electrical properties of the BFO layer and understand the relationship between the ferroelectric polarization and the surface charge distribution, the written domain patterns (the same area as that covered by the PFM measurement) were analyzed using EFM, which is sensitive to the presence of surface charge [10, 18]. It can thus be used to investigate the difference between the surface charge density of domains produced by the same bias with time. The results of the EFM measurements are shown in Figs. 4(a)–(g). During the EFM measurement, a voltage of +3.5 V DC was applied to the conductive tip, which was kept 30 nm above the surface of the BFO layers, at a frequency of 68 kHz [19]. This is op-

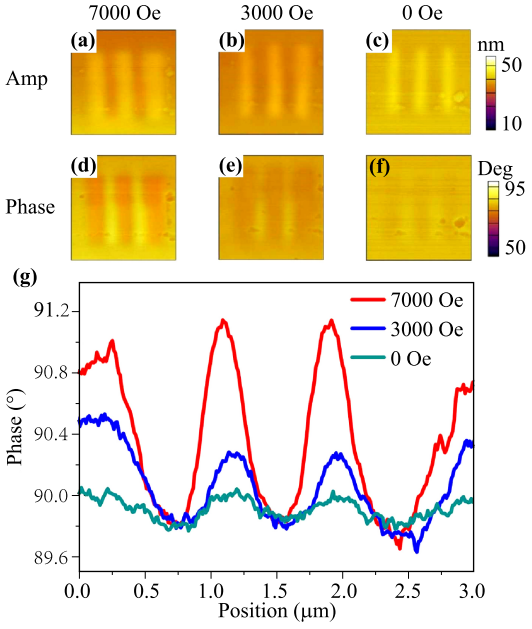

Fig. 4 The amplitudes **(a–c)** and phases **(d–f)** of the EFM images of the BFO layer under the different magnetic fields in the same region. **(g)** Line profiles of the EFM images under the different magnetic fields.

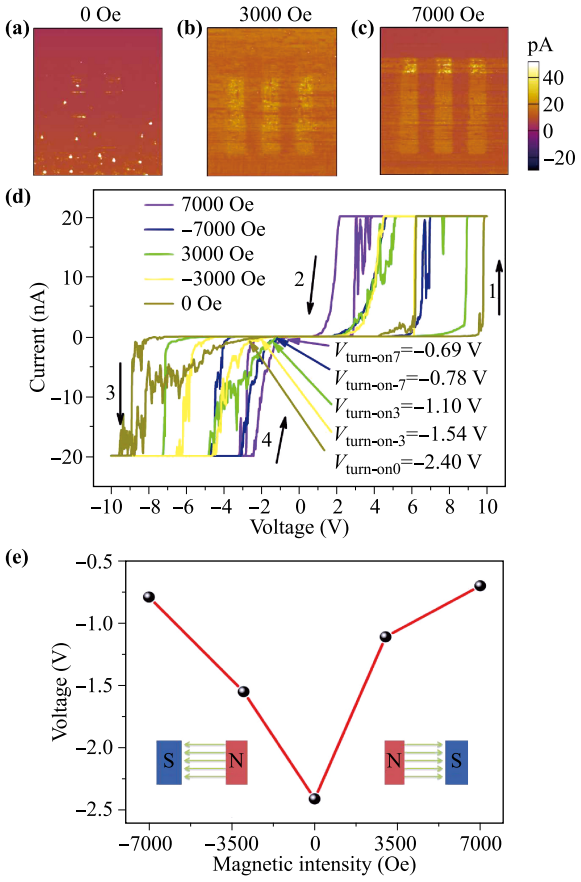

Fig. 5 The current images obtained by CAFM of BFO under the different magnetic fields of **(a)** 0, **(b)** 3000, and **(c)** 7000 Oe. **(d)** The *I–V* curves and **(e)** the turn-on voltage of the as-grown area with the conductive tip as the top electrode under the magnetic field of −7000 Oe → 0 Oe → 7000 Oe.

posite to the negative bound polarization charge of the domains, suggesting that the signal detected by EFM is due to a surface charge that screens the polarization of the downward-oriented domains [20]. This confirmed that the polarization affects the redistribution of surface charges. When the ferroelectric polarization points to the BFO (downward polarization), the positive bound charges at the BFO/NSTO interface will force the electrons on the surface of the NSTO to accumulate. If a positive voltage is applied to the BFO/NSTO heterostructure, the positively polarized bound charges are aggregated at the BFO/NSTO interface. The BFO layer displays a much more obvious contrast for the poled domain on the same scale at $H = 7000$ Oe than at other magnetic field intensities, as shown in Fig. 5(g), indicating that the BFO layer has a high screening charge density at $H = 7000$ Oe. Therefore, the storage density is expected to be higher than that under the other two magnetic intensities under the same conditions. This result provides evidence that the magnetic intensity plays an important role in tuning the surface charge density of the BFO layers. BFO is a multiferroic material, and a spontaneous polarization and an antiferromagnetic state coexist in the BFO bulk. However, a ferromagnetic state will form at the interface of a BFO film deposited on a perovskite substrate, such as $SrTiO_3$ [1]. The spontaneous polarization of the BFO layer on the NSTO substrate produces an internal electric field, which drives the electron motion. This spontaneous polarization would be strongly sensitive to an external magnetic field due to the ferromagnetic state at the interface. In addition, the external magnetic field strengthens the internal electric field, which drives further charge accumulation and slows polarization reversal, thus increasing the retention time.

The local current switching properties and *I–V* curves of the BFO layers under different magnetic fields were also measured via CAFM, as shown in Fig. 5. Figures 5(a)–(c) show that the poled domains with upward polarization have lower conductivity than those with downward polarization. The current contrasts clearly suggest that the local conduction is controlled by polarization reversal, which results in modulation of the barrier height. Upon polarization reversal, the polarization charges are redistributed, resulting in a change in the energy difference at the interface between BFO and NSTO [7]. In addition, their surface features (topography) can be observed from the current images. Three almost invisible vertical lines in the current distribution at $H = 0$

Oe are shown in Fig. 5(a). Three clear vertical lines with a moderate current at $H = 3000$ Oe can be observed in Fig. 5(b), and three reasonably clear vertical lines with a large current at $H = 7000$ Oe appear in Fig. 5(c). The I–V curves were measured by sweeping the voltage from −10 to +10 V, as shown in Fig. 5(d). The tip was positioned in the as-grown areas of the layer using the MFP-3D's "pick a point" force curve interface, with a limited current of 20 nA. Specifically, the conductivity is highest at $H = 7000$ Oe and lowest at 0 Oe. A clear rectifying characteristic and a difference in the leakage current can be observed from the I–V curves. The turn-on voltage is gradually reduced by increasing the magnetic field owing to the migration of carriers under various magnetic fields [21, 22]. In addition, the influence of the magnetic field direction can be neglected, as shown in Fig. 5(e).

Figure 6(a) shows a schematic of the charge distribution at the various interfaces as modulated by the polarization orientation. When the ferroelectric polarization points to the BFO (downward polarization), the positive bound charges at the BFO/NSTO interface will force the electrons on the NSTO surface of to accumulate. If a positive voltage is applied to the BFO/NSTO heterojunction, the positively polarized bound charges are aggregated at the BFO/NSTO interface. These detailed experiments and analyses revealed a gradual reduction of the switching voltage in the BFO/NSTO heterojunction, as shown in Fig. 6(a). It is explained by ferroelectric polarization modulation under the magnetic field. The potential decay length and the height of potential barrier are related to the magnetic field density of the BFO layer. Furthermore, a depletion region was developed by interdiffusion of the majority carriers after dynamic equilibrium was reached. Energy band bending and a potential decay length are also induced by the depletion region. The polarization of the BFO layer can be switched using writing voltage pulses with different directions. Polarization reversal will result in two banding states and corresponding internal electrical fields, thereby changing the barrier height and potential decay length. Incomplete screening of bound charges forms a depolarization field, which is opposite in direction to the polarized electric field in the ferroelectric layer [23]. After a transverse magnetic field is applied, the ferroelectric domain is deflected in the magnetic field, causing the bound charges to migrate. Decomposition of the depolarization field reduces the barrier height and barrier length, illustrated in Fig. 6(b).

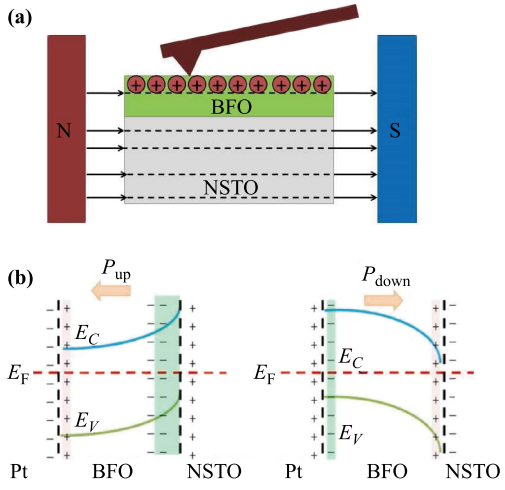

Fig. 6 **(a)** Schematic of experimental set-up. **(b)** Energy-band diagrams of the BFO/NSTO heterojunction with the different polarizations.

In summary, the interfacial state of a ferroelectric semiconductor BFO/NSTO heterojunction was modulated by ferroelectric polarization reversal. The dynamics of surface screening charges on the BFO layer was also investigated by SP measurements. The magnetic intensities are thought to strongly affect the interaction at the BFO/NSTO interface and the energy band configuration. The BFO film exhibits the strongest self-polarization and the largest piezoelectric response. These findings are significant for understanding the role of the magnetic intensity on the properties of BFO films and provide a way to improve the properties of BFO films, or even the performance of devices based on BFO films, by tuning the magnetic field.

Acknowledgements This work was supported by the National Natural Science Foundation of China (Grant No. 11574365).

References

1. J. Wang, J. B. Neaton, H. Zheng, V. Nagarajan, S. B. Ogale, B. Liu, D. Viehland, V. Vaithyanathan, D. G. Schlom, U. V. Waghmare, N. A. Spaldin, K. M. Rabe, M. Wuttig, and R. Ramesh, Epitaxial $BiFeO_3$ multiferroic thin film heterostructures, *Science* 299(5613), 1719 (2003)
2. S. H. Baek, C. M. Folkman, J. W. Park, S. Lee, C. W. Bark, T. Tybell, and C. B. Eom, The nature of polarization fatigue in $BiFeO_3$, *Adv. Mater.* 23(14), 1621 (2011)
3. H. Guo, R. Zhao, K. Jin, L. Gu, D. Xiao, Z. Yang, X. Li, L. Wang, X. He, J. Gu, Q. Wan, C. Wang, H. Lu, C. Ge, M. He, and G. Yang, Interfacial-strain-induced structural and polarization evolutions in epitaxial multiferroic $BiFeO_3$ (001) thin films, *ACS Appl. Mater. Interfaces* 7(4), 2944 (2015)
4. L. Wang, K. J. Jin, J. X. Gu, C. Ma, X. He, J. Zhang, C. Wang, Y. Feng, Q. Wan, J. A. Shi, L. Gu, M. He, H. B. Lu, and G. Z. Yang, A new non-destructive readout by using photo-recovered surface potential contrast, *Sci. Rep.* 4(1), 6980 (2015)

5. J. X. Gu, K. J. Jin, L. Wang, X. He, H. Z. Guo, C. Wang, M. He, and G. Z. Yang, Long-time relaxation of photo-induced influence on $BiFeO_3$ thin films, *J. Appl. Phys.* 118(20), 204103 (2015)
6. T. Yang, X. Zhang, B. Chen, H. Guo, K. Jin, X. Wu, X. Gao, Z. Li, C. Wang, and X. Li, The evidence of giant surface flexoelectric field in (111) oriented $BiFeO_3$ thin film, *ACS Appl. Mater. Interfaces* 9(6), 5600 (2017)
7. B. C. Jeon, D. Lee, M. H. Lee, S. M. Yang, S. C. Chae, T. K. Song, S. D. Bu, J. S. Chung, J. G. Yoon, and T. W. Noh, Flexoelectric effect in the reversal of self-polarization and associated changes in the electronic functional properties of $BiFeO_3$ thin films, *Adv. Mater.* 25(39), 5643 (2013)
8. R. Guo, L. You, M. Motapothula, Z. Zhang, M. B. H. Breese, L. Chen, D. Wu, and J. L. Wang, Influence of target composition and deposition temperature on the domain structure of $BiFeO_3$ thin films, *AIP Adv.* 2(4), 042104 (2012)
9. J. C. Yang, Q. He, P. Yu, and Y. H. Chu, $BiFeO_3$ thin films: A playground for exploring electric-field control of multifunctionalities, *Annu. Rev. Mater. Res.* 45(1), 249 (2015)
10. Y. Yang, I. C. Infante, B. Dkhil, and L. Bellaiche, Strain effects on multiferroic $BiFeO_3$ films, *Comp. Rend. Phys.* 16(2), 193 (2015)
11. Z. Gao, X. Huang, P. Li, L. Wang, L. Wei, W. Zhang, and H. Guo, Reversible resistance switching of 2D electron gas at $LaAlO_3/SrTiO_3$ heterointerface, *Adv. Mater. Interfaces* 5(8), 1701565 (2018)
12. X. Huang, Z. Gao, P. Li, L. Wang, X. Liu, W. Zhang, and H. Guo, Resistance change effect in $SrTiO_3$/Si(001) isotype heterojunction, *J. Appl. Phys.* 123(8), 084502 (2018)
13. P. Sharma, Y. Heo, B. K. Jang, Y. Y. Liu, J. Y. Li, C. H. Yang, and J. Seidel, Structural and electronic transformation pathways in morphotropic $BiFeO_3$, *Sci. Rep.* 6(1), 32347 (2016)
14. C. Wang, K. J. Jin, Z. T. Xu, L. Wang, C. Ge, H. B. Lu, H. Z. Guo, M. He, and G. Z. Yang, Switchable diode effect and ferroelectric resistive switching in epitaxial $BiFeO_3$ thin films, *Appl. Phys. Lett.* 98(19), 192901 (2011)
15. C. Beekman, W. Siemons, M. Chi, N. Balke, J. Y. Howe, T. Z. Ward, P. Maksymovych, J. D. Budai, J. Z. Tischler, R. Xu, W. Liu, and H. M. Christen, Ferroelectric self-poling, switching, and monoclinic domain configuration in $BiFeO_3$ thin films, *Adv. Funct. Mater.* 26(28), 5166 (2016)
16. Y. L. Huang, W. S. Chang, C. N. Van, H. J. Liu, K. A. Tsai, J. W. Chen, H. H. Kuo, W. Y. Tzeng, Y. C. Chen, C. L. Wu, C. W. Luo, Y. J. Hsu, and Y. H. Chu, Tunable photoelectrochemical performance of Au/$BiFeO_3$ heterostructure, *Nanoscale* 8(34), 15795 (2016)
17. J. H. Lee, I. Fina, X. Marti, Y. H. Kim, D. Hesse, and M. Alexe, Spintronic functionality of $BiFeO_3$ domain walls, *Adv. Mater.* 26(41), 7078 (2014)
18. Y. Zhou, L. Fang, L. You, P. Ren, L. Wang, and J. L. Wang, Photovoltaic property of domain engineered epitaxial $BiFeO_3$ films, *Appl. Phys. Lett.* 105(25), 252903 (2014)
19. F. Bi, M. Huang, H. Lee, C. B. Eom, P. Irvin, and J. Levy, $LaAlO_3$ thickness window for electronically controlled magnetism at $LaAlO_3/SrTiO_3$ heterointerfaces, *Appl. Phys. Lett.* 107(8), 082402 (2015)
20. M. Trassin, G. D. Luca, S. Manz, and M. Fiebig, Probing ferroelectric domain engineering in $BiFeO_3$ thin films by second harmonic generation, *Adv. Mater.* 27(33), 4871 (2015)
21. Q. Li, Y. Cao, P. Yu, R. K. Vasudevan, N. Laanait, A. Tselev, F. Xue, L. Q. Chen, P. Maksymovych, S. V. Kalinin, and N. Balke, Giant elastic tunability in strained $BiFeO_3$ near an electrically induced phase transition, *Nat. Commun.* 6(1), 8985 (2015)
22. H. Guo, Q. Li, Z. Yang, K. J. Jin, C. Ge, L. Gu, X. He, X. Li, R. Zhao, Q. Wan, J. Wang, M. He, C. Wang, H. Lu, Y. Yang, and G. Yang, Manipulating magnetoelectric properties by interfacial coupling in $La_{0.3}Sr_{0.7}MnO_3/Ba_{0.7}Sr_{0.3}TiO_3$ superlattices, *Sci. Rep.* 7(1), 7693 (2017)
23. R. Huang, H. C. Ding, W. I. Liang, Y. C. Gao, X. D. Tang, Q. He, C. G. Duan, Z. Zhu, J. Chu, C. A. J. Fisher, T. Hirayama, Y. Ikuhara, and Y. H. Chu, Atomic-scale visualization of polarization pinning and relaxation at coherent $BiFeO_3/LaAlO_3$ interfaces, *Adv. Funct. Mater.* 24(6), 793 (2014)